Frontiers of Information Technology & Electronic Engineering
www.jzus.zju.edu.cn; engineering.cae.cn; www.springerlink.com
ISSN 2095-9184 (print); ISSN 2095-9230 (online)
E-mail: jzus@zju.edu.cn

A comprehensive error calibration method based on dual uniform circular array

Jia-jia ZHANG[†‡], Hui CHEN, Song XIAO, Meng-yu NI

Air Force Early Warning Academy, Wuhan 430019, China

[†]E-mail: zjj2015wuhan@163.com

Received Apr. 16, 2018; Revision accepted Oct. 22, 2018; Crosschecked Sept. 4, 2019

Abstract: Based on the dual uniform circular array, a novel method is proposed to estimate the direction-of-arrival (DOA) and jointly calibrate gain-phase errors, position errors, and mutual coupling errors. In this paper, only one auxiliary source is required to generate three time-disjoint calibration sources with the help of the rotation platform. Subsequently, according to the principle that the signal subspace is orthogonal to the noise subspace, the cost function is constructed. The alternating iteration method is used to estimate the coefficients of the three kinds of errors. During the process, the proposed algorithm makes full use of the structural characteristics of the array when estimating mutual coupling errors, while the signal phase matrix is used to eliminate the phase influence caused by the delay in signal arrival at the antenna array when estimating gain-phase errors and position errors. Compared with the algorithm using multidimensional nonlinear search, the proposed algorithm has lower computational complexity. Moreover, our algorithm does not require additional auxiliary sensors. Simulation results demonstrate that the proposed algorithm is effective and can precisely and comprehensively calibrate the errors in a dual uniform circular array.

Key words: Dual uniform circular array; Gain-phase errors; Position errors; Mutual coupling errors; Calibration
https://doi.org/10.1631/FITEE.1800240 **CLC number:** TN911.7

1 Introduction

As one of the most common two-dimensional (2D) arrays, the uniform circular array (UCA) (Belfiori et al., 2012; Wu et al., 2016) has been widely used in practical applications. Like the UCA, the dual uniform circular array has many advantages. The dual uniform circular array can provide 360° omnidirectional and unambiguous 2D angular information (Zhang et al., 2018). It has the same estimation accuracy and resolution in any direction. Additionally, with the same number of array elements, the sidelobe level of the dual uniform circular array is lower than that of the UCA. Therefore, the interference from the sidelobe can be effectively prevented and the anti-interference ability can be improved. As a result, study on dual uniform circular arrays is of great significance. In actual applications, the direction-of-arrival (DOA) estimation will not be carried out under completely ideal conditions. The existence of errors will directly result in the reduction of performance or even failure of the high resolution algorithms (Friedlander and Weiss, 1991; Cheng et al., 2017). How to effectively calibrate the array errors has always been of special interest in array signal processing.

So far, many kinds of methods have been used to calibrate array errors. These methods can be roughly divided into two categories: self-calibration class (Sellone and Serra, 2007; Wang D, 2015; Wang M et al., 2015; Guo et al., 2017) and active calibration class (Jia et al., 1996; Ng and See, 1996; Hu, 2009; Wang D, 2011, 2015; Yuan et al., 2014; Li et al., 2016; Liu et al., 2016). Nowadays, active calibration methods are the main methods to comprehensively calibrate errors. Gain-phase errors and mutual coupling errors were jointly calibrated in Hu (2009),

‡ Corresponding author
ORCID: Jia-jia ZHANG, http://orcid.org/0000-0001-8793-7872

Wang D (2011), Li et al. (2016), and Liu et al. (2016). In Hu (2009), both auxiliary sources and auxiliary sensors were used, which increases the cost. Additionally, the method requires that the array error cannot be too large. In Liu et al. (2016), the mutual coupling matrix with cyclic symmetric characteristics can be represented as the product of the Fourier matrix and the diagonal matrix. The linear relationship between the gain-phase errors and the vector formed by the diagonal matrix was found. Then, decoupling of the two errors was completed. The method requires no iteration, and hence the computational complexity is small. However, it has special requirements for the structure of the array. The method in Li et al. (2016) has an advantage in low signal-to-noise ratio (SNR) conditions, but it does not perform well when the angles of the calibrated sources are close. In Wang D (2011), the unknown parameters can be reduced, but the precise angles of the auxiliary sources should be known first. In Jia et al. (1996) and Yuan et al. (2014), gain-phase errors and position errors were jointly calibrated. The main difference between the two methods is that the former needs to be applied at high SNR. Ng and See (1996) and Wang and Wu (2015) proposed joint calibration methods for gain-phase errors, position errors, and mutual coupling errors. The maximum likelihood algorithm was used in Ng and See (1996). However, the mutual coupling property is not considered in this method. Therefore, the calculation is complicated and the estimation accuracy is low. Wang (2015) designed numerical algorithms to compensate for the array distortion matrix, especially for the uniform linear array and UCA. The algorithm takes full advantage of the special structure of the array and has high estimation performance. However, it requires a set of time-disjoint auxiliary sources at known locations. The accuracy of the auxiliary sources has a great influence on the algorithm.

In this paper, aimed at the dual uniform circular array, a joint calibration method is proposed to deal with gain-phase errors, position errors, and mutual coupling errors. The method can estimate the DOAs of the incoherent sources and the coefficients of the three kinds of errors. First, three independent time-disjoint signal sources are obtained with the help of the rotation platform. After obtaining the sample data from the three calibration sources, the cost function is constructed using the orthogonal relationship between the signal subspace and the noise subspace. Then, an alternating iteration method is used to obtain the error coefficients. In this way, the three kinds of array error matrices can be restored. Finally, the MUSIC algorithm is used to estimate the DOAs of the signals. During the iterative process to obtain the error coefficients, the algorithm makes full use of the Toeplitz characteristics of partitioned mutual coupling matrices. Furthermore, the signal phase matrix is used to eliminate the phase effect caused by the delay in signal arrival at the antenna array. No additional auxiliary sensors are needed, so there is no increase in cost. Simulation results show that the algorithm can effectively estimate the directions of the signals and solve the problem of comprehensive error calibration for the dual uniform circular array.

Notations: Upper- and lower-case letters in bold denote matrices and vectors, respectively. $\boldsymbol{X}^{\mathrm{T}}$, $\boldsymbol{X}^{\mathrm{H}}$, and $\boldsymbol{X}^{*}$ represent the operations of transpose, Hermitian transpose, and complex conjugate, respectively. $\lceil\kappa\rceil$ denotes the smallest integer larger than κ. Span$\{\boldsymbol{X}\}$ represents the subspace spanned by $\boldsymbol{X}$. $\|\boldsymbol{X}\|_{\mathrm{F}}$ denotes the Frobenius norm of matrix $\boldsymbol{X}$. $\boldsymbol{C}^{M\times N}$ denotes an $M\times N$ complex matrix. "•" stands for the Khatri-Rao product. $\boldsymbol{E}$ represents an all-1 matrix. angle($\boldsymbol{X}$) denotes the operation for obtaining the phase angle of matrix $\boldsymbol{X}$. diag($\boldsymbol{x}$) represents a diagonal matrix that uses the elements of vector $\boldsymbol{x}$ as its diagonal elements.

2 Data model for the dual uniform circular array

2.1 Array structure

The array used in this work is shown in Fig. 1. In the XOY plane, $2N$ omni-directional array elements are evenly distributed on two concentric circles centered at the origin. The radius of the inner circle is r_1, and the number of elements is N. The radius of the outer circle is r_2, and the number of array elements is also N. The position of the $\bar{k}^{\mathrm{th}}$ element in the array can be expressed as

$$x_{\bar{k}}=\begin{cases} r_1\cos\left[\dfrac{2\pi}{N}(\bar{k}-1)\right], & 1\le\bar{k}\le N,\\ r_2\cos\left[\dfrac{2\pi}{N}(\bar{k}-1)\right], & N+1\le\bar{k}\le 2N, \end{cases} \tag{1}$$

$$y_{\bar{k}}=\begin{cases} r_1\sin\left[\dfrac{2\pi}{N}(\bar{k}-1)\right], & 1\le\bar{k}\le N, \\ r_2\sin\left[\dfrac{2\pi}{N}(\bar{k}-1)\right], & N+1\le\bar{k}\le 2N. \end{cases} \tag{2}$$

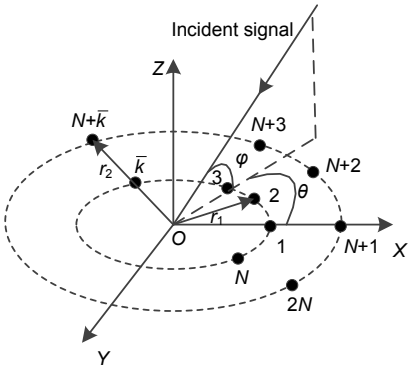

Fig. 1 Array structure

For convenience, only the azimuth angle θ is considered, $\theta\in[-180°, 180°]$. Taking the origin as the reference point, the steering vector can be expressed as

$$\boldsymbol{a}(\theta_i)=\exp\left(-\mathrm{j}\frac{2\pi}{\lambda}[\boldsymbol{x},\boldsymbol{y}][\sin\theta_i,\cos\theta_i]^{\mathrm{T}}\right), \tag{3}$$

where $[\boldsymbol{x},\boldsymbol{y}]$ represents the position matrix with $2N\times2$ dimensions. Then, the array manifold matrix without array errors can be expressed as

$$\boldsymbol{A}=\left[\boldsymbol{a}(\theta_1),\boldsymbol{a}(\theta_2),...,\boldsymbol{a}(\theta_M)\right], \tag{4}$$

where M indicates the number of sources.

2.2 Data model in the presence of comprehensive errors

When the gain-phase errors, position errors, and mutual coupling errors coexist, the received data $\boldsymbol{X}$ of the array can be expressed as

$$\boldsymbol{X}(t)=\bar{\boldsymbol{A}}(\theta)\boldsymbol{S}(t)+\boldsymbol{N}(t)=\boldsymbol{ZGV}(\theta)\boldsymbol{S}(t)+\boldsymbol{N}(t), \tag{5}$$

where $\bar{\boldsymbol{A}}(\theta)$ denotes the array manifold matrix in the presence of comprehensive errors, $\boldsymbol{S}(t)=[s_1(t), s_2(t), \ldots, s_M(t)]^{\mathrm{T}}$ is the signal vector, and $\boldsymbol{N}(t)=[n_1(t), n_2(t), \ldots, n_{2N}(t)]^{\mathrm{T}}$ is the white Gaussian noise vector with zero mean. $\boldsymbol{Z}$ denotes the mutual coupling matrix, $\boldsymbol{G}$ denotes the gain-phase error matrix, and $\boldsymbol{V}(\theta)$ denotes the array manifold matrix in the presence of position errors.

According to the structure of the dual uniform circular array in Fig. 1, the mutual coupling matrix $\boldsymbol{Z}$ can be partitioned as follows:

$$\boldsymbol{Z}=\begin{bmatrix}\boldsymbol{D}_1 & \boldsymbol{B}\\ \boldsymbol{B} & \boldsymbol{D}_2\end{bmatrix}, \tag{6}$$

where $\boldsymbol{D}_1$ and $\boldsymbol{D}_2$ represent the mutual coupling matrix of the inner and outer circular arrays, respectively, and $\boldsymbol{B}$ represents the mutual coupling matrix between two circular arrays. According to Zhang et al. (2017), we know that all of matrices $\boldsymbol{D}_1$, $\boldsymbol{D}_2$, and $\boldsymbol{B}$ have cyclic banded symmetric Toeplitz characteristics. They can be uniquely described by the nonzero elements of their first row. Assume that there are p nonzero elements in the first row of $\boldsymbol{D}_1$, which can be denoted by $\boldsymbol{g}=[g_1, g_2, \ldots, g_p]^{\mathrm{T}}$, $g_1=1$. There are k nonzero elements in the first row of $\boldsymbol{D}_2$, which can be denoted by $\boldsymbol{d}=[d_1, d_2, \ldots, d_k]^{\mathrm{T}}$, $d_1=1$. There are also q nonzero elements in the first line of $\boldsymbol{B}$, which can be denoted by $\boldsymbol{b}=[b_1, b_2, \ldots, b_q]^{\mathrm{T}}$, $b_1\neq1$.

Thus, the maximum distance with which a mutual coupling can exist between two elements in the inner circular array can be expressed as

$$d_1=\sqrt{r_1^2+r_1^2-2r_1r_1\cos\left[(p-1)2\pi/N\right]}. \tag{7}$$

The maximum distance with which a mutual coupling can exist between an element in the inner circular array and an element in the outer circular array can be expressed as

$$d_2=\sqrt{r_1^2+r_2^2-2r_1r_2\cos\left[(q-1)2\pi/N\right]}. \tag{8}$$

The maximum distance with which a mutual coupling can exist between two elements in the outer circular array can be expressed as

$$d_3=\sqrt{r_2^2+r_2^2-2r_2r_2\cos\left[(k-1)2\pi/N\right]}. \tag{9}$$

In general, the larger the distance between neighboring elements, the weaker the effect of mutual coupling. Thus, the following relationships hold true:

$$d_1\le2r_1,\ d_2\le d_1,\ d_3\le d_1. \tag{10}$$

Substituting Eqs. (7)–(9) into inequality (10) yields

$$1 \le p \le \lceil N/2 \rceil,\ 0 \le q < p,\ 1 \le k < p. \tag{11}$$

Only when the mutual coupling does not exist, p=k=1, is q=0 established. According to the above analysis, the mutual coupling coefficient vector $\boldsymbol{z}$ can be expressed as

$$\boldsymbol{z} = \left[\boldsymbol{g}^{\mathrm{T}}, \boldsymbol{d}^{\mathrm{T}}, \boldsymbol{b}^{\mathrm{T}}\right]^{\mathrm{T}},\ z(1) = 1. \tag{12}$$

According to Wang et al. (2004), the gain-phase errors are usually modeled by a diagonal matrix

$$\boldsymbol{G} = \mathrm{diag}\left(\rho_1 \mathrm{e}^{\mathrm{j}\phi_1}, \rho_2 \mathrm{e}^{\mathrm{j}\phi_2}, \cdots, \rho_{2N} \mathrm{e}^{\mathrm{j}\phi_{2N}}\right), \tag{13}$$

where ρ_i and ϕ_i are the gain and phase perturbations of the i^{th} element, respectively. Usually, the first element in the array is used as a reference element, ρ_1=1, ϕ_1=0.

When the position errors exist, the position disturbance matrix $[\Delta\boldsymbol{x}, \Delta\boldsymbol{y}]$ is added based on the ideal position matrix. Therefore, the steering vector in the presence of position errors can be expressed as

$$\begin{aligned}\boldsymbol{v}(\theta_i) &= \exp\left(-\mathrm{j}2\pi[\boldsymbol{x}+\Delta\boldsymbol{x}, \boldsymbol{y}+\Delta\boldsymbol{y}]\begin{bmatrix}\sin\theta_i\\ \cos\theta_i\end{bmatrix}\right)\\ &= \exp\left(-\mathrm{j}2\pi[\boldsymbol{x}, \boldsymbol{y}]\begin{bmatrix}\sin\theta_i\\ \cos\theta_i\end{bmatrix}\right)\\ &\quad\cdot\exp\left(-\mathrm{j}2\pi[\Delta\boldsymbol{x}, \Delta\boldsymbol{y}]\begin{bmatrix}\sin\theta_i\\ \cos\theta_i\end{bmatrix}\right)\\ &= \boldsymbol{a}(\theta_i)\cdot\boldsymbol{h}(\theta_i) = \boldsymbol{H}(\theta_i)\boldsymbol{a}(\theta_i),\ i = 1,2,\cdots,M,\end{aligned} \tag{14}$$

where $\boldsymbol{H}(\theta_i)$=diag($\boldsymbol{h}(\theta_i)$) denotes the position error matrix. Similarly, since the first array element is used as the reference element, there will be $[\Delta x_1, \Delta y_1]$=[0, 0]. The array manifold matrix in the presence of position errors can be modified as

$$\boldsymbol{V}(\theta) = \left[\boldsymbol{v}(\theta_1), \boldsymbol{v}(\theta_2), \cdots, \boldsymbol{v}(\theta_M)\right]. \tag{15}$$

Thus, the covariance matrix of the array in the presence of the comprehensive range of errors can be expressed as

$$\boldsymbol{R} = E[\boldsymbol{X}(t)\boldsymbol{X}^{\mathrm{H}}(t)] = \sigma_{\mathrm{s}}^2\boldsymbol{ZGVV}^{\mathrm{H}}\boldsymbol{G}^{\mathrm{H}}\boldsymbol{Z}^{\mathrm{H}} + \sigma_{\mathrm{n}}^2\boldsymbol{I}, \tag{16}$$

where σ_{s}^2 indicates the source power and σ_{n}^2 the noise power. Due to the limited number of snapshots, the covariance matrix can be calculated by

$$\hat{\boldsymbol{R}} = \frac{1}{L}\sum_{t=1}^{L}\boldsymbol{X}(t)\boldsymbol{X}^{\mathrm{H}}(t), \tag{17}$$

where L denotes the number of snapshots.

3 Description of the algorithm for comprehensive error calibration

3.1 Algorithm principle

Consider that there is an auxiliary source in the far field impinging on the array. The array antenna is placed on a high-precision rotation platform. The antenna is rotated twice continuously. The angle intervals can be obtained according to the records of the rotation platform. The three angles θ_1, θ_2, and θ_3 can be considered three independent time-disjoint signal sources. At the same time, the received data of each angle is recorded during this process. Combining the received data of the three calibrated sources, the covariance matrices $\hat{\boldsymbol{R}}^i$ (i=1, 2, 3) are calculated in turn. $\hat{\boldsymbol{R}}^i$ (i=1, 2, 3) are eigen-decomposed to obtain the corresponding noise subspace $\hat{\boldsymbol{E}}_N^i$ (i=1, 2, 3). According to the subspace theory, the following relationship holds true:

$$\mathrm{span}\left\{\hat{\boldsymbol{E}}_N^i\right\} \perp \mathrm{span}\left\{\boldsymbol{ZGV}(\theta_i)\right\},\ i = 1,2,3. \tag{18}$$

Thus, the cost function can be constructed as

$$J = \sum_{i=1}^{3}\left\|(\hat{\boldsymbol{E}}_N^i)^{\mathrm{H}}\,\overline{\boldsymbol{A}}(\theta_i)\right\|_{\mathrm{F}}^2 = \sum_{i=1}^{3}\left\|(\hat{\boldsymbol{E}}_N^i)^{\mathrm{H}}\,\boldsymbol{ZGv}(\theta_i)\right\|_{\mathrm{F}}^2. \tag{19}$$

It is evident that the cost function J can have the minimum value when the DOAs and the error parameters are accurately estimated. Therefore, the alternating iteration method can be used to estimate the coefficients of mutual coupling errors, gain-phase errors, and position errors in turn. A set of unknown parameters is defined as $f(\boldsymbol{z}, \boldsymbol{\rho}, [\Delta\boldsymbol{x}, \Delta\boldsymbol{y}], \boldsymbol{\phi})$.

At first this method needs to determine the initial value of the iteration. Assume that the number of

iterations l equals 1. The gain-phase error matrix is considered to be an identity matrix, while the position error matrix is a null matrix, i.e., $\boldsymbol{G}=\boldsymbol{I}$, $[\Delta \boldsymbol{x}, \Delta \boldsymbol{y}]=[\boldsymbol{0}, \boldsymbol{0}]$.

1. Estimation of mutual coupling error coefficients $f(\hat{\boldsymbol{z}}, \boldsymbol{\rho}, [\Delta \boldsymbol{x}, \Delta \boldsymbol{y}], \boldsymbol{\phi})$

First, the mutual coupling coefficients are optimized while other parameters remain unchanged. Based on the subspace theory, the cost function can be modified as

$$J=\sum_{i=1}^{3}\left\|(\hat{\boldsymbol{E}}_N^i)^{\mathrm{H}}\boldsymbol{Z}\boldsymbol{G}\boldsymbol{v}(\theta_i)\right\|_{\mathrm{F}}^2=\sum_{i=1}^{3}\left\|(\hat{\boldsymbol{E}}_N^i)^{\mathrm{H}}\boldsymbol{Z}\boldsymbol{w}(\theta_i)\right\|_{\mathrm{F}}^2, \quad (20)$$

where $\boldsymbol{w}(\theta_i)=\boldsymbol{G}\boldsymbol{v}(\theta_i)$. For convenience, θ_i is omitted in the following proof. $\boldsymbol{w}$ can be divided into two parts, namely $\boldsymbol{w}=\begin{bmatrix}\boldsymbol{w}_1\\ \boldsymbol{w}_2\end{bmatrix}$, where $\boldsymbol{w}_1$ denotes the former N elements of $\boldsymbol{w}$ and $\boldsymbol{w}_2$ denotes the latter N elements of $\boldsymbol{w}$. Combining Eq. (6), $\boldsymbol{Z}\boldsymbol{w}$ can be expressed as

$$\boldsymbol{Z}\boldsymbol{w}=\begin{bmatrix}\boldsymbol{D}_1 & \boldsymbol{B}\\ \boldsymbol{B} & \boldsymbol{D}_2\end{bmatrix}\begin{bmatrix}\boldsymbol{w}_1\\ \boldsymbol{w}_2\end{bmatrix}=\begin{bmatrix}\boldsymbol{D}_1\boldsymbol{w}_1+\boldsymbol{B}\boldsymbol{w}_2\\ \boldsymbol{B}\boldsymbol{w}_1+\boldsymbol{D}_2\boldsymbol{w}_2\end{bmatrix}. \quad (21)$$

Since $\boldsymbol{D}_1$, $\boldsymbol{D}_2$, and $\boldsymbol{B}$ have banded symmetric Toeplitz characteristics, we have

$$\boldsymbol{D}_1\boldsymbol{w}_1=\boldsymbol{T}[\boldsymbol{w}_1]\boldsymbol{g}, \quad (22)$$

$$\boldsymbol{D}_2\boldsymbol{w}_2=\boldsymbol{T}[\boldsymbol{w}_2]\boldsymbol{d}, \quad (23)$$

$$\boldsymbol{B}\tilde{\boldsymbol{w}}=\boldsymbol{T}[\tilde{\boldsymbol{w}}]\boldsymbol{b}, \quad (24)$$

where $\tilde{\boldsymbol{w}}=\boldsymbol{w}_1$ or $\boldsymbol{w}_2$, and $\boldsymbol{T}[\tilde{\boldsymbol{w}}]$ can be specifically expressed as

$$\boldsymbol{T}[\tilde{\boldsymbol{w}}]=\boldsymbol{T}_1[\tilde{\boldsymbol{w}}]+\boldsymbol{T}_2[\tilde{\boldsymbol{w}}]+\boldsymbol{T}_3[\tilde{\boldsymbol{w}}]+\boldsymbol{T}_4[\tilde{\boldsymbol{w}}], \quad (25)$$

$$T_1(i,j)=\begin{cases}\tilde{w}_{(\theta)}(i+j-1), & i+j\le N+1,\\ 0, & \text{otherwise},\end{cases} \quad (26)$$

$$T_2(i,j)=\begin{cases}\tilde{w}_{(\theta)}(i-j+1), & i\ge j\ge 2,\\ 0, & \text{otherwise},\end{cases} \quad (27)$$

$$T_3(i,j)=\begin{cases}\tilde{w}_{(\theta)}(i-j+N+1), & i<j\le p,\\ 0, & \text{otherwise},\end{cases} \quad (28)$$

$$T_4(i,j)=\begin{cases}\tilde{w}_{(\theta)}(i-j-N-1),\\ \quad i+j\ge N+2, p\ge j\ge 2,\\ 0, \quad \text{otherwise},\end{cases} \quad (29)$$

where $\tilde{w}_{(\theta)}(i+j-1)$ represents the $(i+j-1)^{\text{th}}$ element of $\tilde{\boldsymbol{w}}$. Substituting Eqs. (22)–(29) into Eq. (21) yields

$$\begin{aligned}\boldsymbol{Z}\boldsymbol{w}&=\begin{bmatrix}\boldsymbol{T}[\boldsymbol{w}_1]\boldsymbol{g}+\boldsymbol{T}[\boldsymbol{w}_2]\boldsymbol{b}\\ \boldsymbol{T}[\boldsymbol{w}_1]\boldsymbol{b}+\boldsymbol{T}[\boldsymbol{w}_2]\boldsymbol{d}\end{bmatrix}\\ &=\begin{bmatrix}\boldsymbol{T}[\boldsymbol{w}_1] & \boldsymbol{0}_{N\times k} & \boldsymbol{T}[\boldsymbol{w}_2]\\ \boldsymbol{0}_{N\times p} & \boldsymbol{T}[\boldsymbol{w}_2] & \boldsymbol{T}[\boldsymbol{w}_1]\end{bmatrix}\begin{bmatrix}\boldsymbol{g}\\ \boldsymbol{d}\\ \boldsymbol{b}\end{bmatrix}=\boldsymbol{T}[\boldsymbol{w}]\hat{\boldsymbol{z}},\end{aligned} \quad (30)$$

where $\hat{\boldsymbol{z}}$ represents the estimation vector of mutual coupling coefficients. Substituting Eq. (30) into Eq. (20), J can be rewritten as

$$\begin{aligned}J&=\sum_{i=1}^{3}\left(\boldsymbol{T}[\boldsymbol{w}(\theta_i)]\hat{\boldsymbol{z}}\right)^{\mathrm{H}}\hat{\boldsymbol{E}}_N^i\left(\hat{\boldsymbol{E}}_N^i\right)^{\mathrm{H}}\boldsymbol{T}[\boldsymbol{w}(\theta_i)]\hat{\boldsymbol{z}}\\ &=\hat{\boldsymbol{z}}^{\mathrm{H}}\left\{\sum_{i=1}^{3}\left(\boldsymbol{T}[\boldsymbol{w}(\theta_i)]\right)^{\mathrm{H}}\hat{\boldsymbol{E}}_N^i\left(\hat{\boldsymbol{E}}_N^i\right)^{\mathrm{H}}\boldsymbol{T}[\boldsymbol{w}(\theta_i)]\right\}\hat{\boldsymbol{z}}\\ &=\hat{\boldsymbol{z}}^{\mathrm{H}}\boldsymbol{Q}_1\hat{\boldsymbol{z}},\end{aligned} \quad (31)$$

$$\boldsymbol{Q}_1=\sum_{i=1}^{3}\left(\boldsymbol{T}[\boldsymbol{w}(\theta_i)]\right)^{\mathrm{H}}\hat{\boldsymbol{E}}_N^i\left(\hat{\boldsymbol{E}}_N^i\right)^{\mathrm{H}}\boldsymbol{T}[\boldsymbol{w}(\theta_i)]. \quad (32)$$

Usually, the first element in $\boldsymbol{z}$ is 1. Set the line constraint $\boldsymbol{W}_1^{\mathrm{T}}\boldsymbol{z}=1$, where $\boldsymbol{W}_1=[1, 0, 0, \ldots, 0]^{\mathrm{T}}\in C^{(p+k+q)\times 1}$. Thus, using the method of Lagrange multipliers, the optimization solution of $\boldsymbol{z}$ is derived as

$$\hat{\boldsymbol{z}}=\frac{(\boldsymbol{Q}_1)^{-1}\boldsymbol{W}_1}{\boldsymbol{W}_1^{\mathrm{T}}(\boldsymbol{Q}_1)^{-1}\boldsymbol{W}_1}. \quad (33)$$

According to the structure of the dual uniform circular array, the mutual coupling matrix $\hat{\boldsymbol{Z}}$ can be reconstructed by the estimated mutual coupling coefficient vector $\hat{\boldsymbol{z}}$.

2. Estimation of gain error coefficients $f\left(\boldsymbol{z}, \hat{\boldsymbol{\rho}}, [\Delta \boldsymbol{x}, \Delta \boldsymbol{y}], \boldsymbol{\phi}\right)$

Second, the gain error coefficients are optimized while the mutual coupling matrix $\hat{\boldsymbol{Z}}$ as a known parameter remains unchanged. Inserting $\hat{\boldsymbol{Z}}$ into $\hat{\boldsymbol{R}}^i$ (i=1, 2, 3) yields

$$\hat{\boldsymbol{R}}^i=\hat{\boldsymbol{Z}}^{-1}\left(\hat{\boldsymbol{R}}^i-\sigma_{\mathrm{n}}^2\boldsymbol{I}\right)\left(\hat{\boldsymbol{Z}}^{\mathrm{H}}\right)^{-1}=\sigma_{\mathrm{s}}^2\boldsymbol{G}\boldsymbol{v}(\theta_i)\left[\boldsymbol{v}(\theta_i)\right]^{\mathrm{H}}\boldsymbol{G}^{\mathrm{H}}. \quad (34)$$

If the gain-phase error matrix and the position error matrix are considered as a whole, the new diagonal matrix $\boldsymbol{\Gamma}^i$ can be expressed as

$$\boldsymbol{\Gamma}^i=\mathrm{diag}\left(1,\rho_2\mathrm{e}^{\mathrm{j}\phi_2}\exp\left(-\mathrm{j}\frac{2\pi}{\lambda}\left(\Delta x_2\sin\theta_i+\Delta y_2\cos\theta_i\right)\right),\cdots,\rho_{2N}\mathrm{e}^{\mathrm{j}\phi_{2N}}\exp\left(-\mathrm{j}\frac{2\pi}{\lambda}\left(\Delta x_{2N}\sin\theta_i+\Delta y_{2N}\cos\theta_i\right)\right)\right),\quad i=1,2,3. \tag{35}$$

The phase information is extracted. We have

$$\varphi_n=\phi_n-\frac{2\pi}{\lambda}\left(\Delta x_n\sin\theta_i+\Delta y_n\cos\theta_i\right),\ n=1,2,\cdots,2N. \tag{36}$$

It is known from Jin et al. (2010) that the signal phase matrix can be constructed to eliminate the phase influence caused by the delay of the signal reaching the antenna. Thus, set $\boldsymbol{R}^i_{\mathrm{ideal}}=\boldsymbol{a}(\theta_i)(\boldsymbol{a}(\theta_i))^{\mathrm{H}}$ (i=1, 2, 3), and we have

$$\begin{aligned}\boldsymbol{B}^i&=\hat{\boldsymbol{R}}^i\cdot\left(\boldsymbol{R}^i_{\mathrm{ideal}}\right)^*\\&=\boldsymbol{\Gamma}^i\sigma_{\mathrm{s}}^2\left[\boldsymbol{a}(\theta_i)(\boldsymbol{a}(\theta_i))^{\mathrm{H}}\right]\left(\boldsymbol{\Gamma}^i\right)^{\mathrm{H}}\cdot\left[\boldsymbol{a}(\theta_i)(\boldsymbol{a}(\theta_i))^{\mathrm{H}}\right]^*\\&=\boldsymbol{\chi}^i\left(\boldsymbol{\chi}^i\right)^{\mathrm{H}}\cdot\left[\sigma_{\mathrm{s}}^2\boldsymbol{a}(\theta_i)(\boldsymbol{a}(\theta_i))^{\mathrm{H}}\right]\cdot\left[\boldsymbol{a}(\theta_i)(\boldsymbol{a}(\theta_i))^{\mathrm{H}}\right]^*\\&=\boldsymbol{\chi}^i\left(\boldsymbol{\chi}^i\right)^{\mathrm{H}}\cdot\sigma_{\mathrm{s}}^2\boldsymbol{E}=\sigma_{\mathrm{s}}^2\boldsymbol{\chi}^i\left(\boldsymbol{\chi}^i\right)^{\mathrm{H}},\end{aligned} \tag{37}$$

where $\boldsymbol{\chi}^i=\mathrm{diag}(\boldsymbol{\Gamma}^i)$ stands for stacking the diagonal elements into a column vector. Obviously, the gain information is contained in the diagonal of $\boldsymbol{B}^i$. Thus, the gain error coefficients can be obtained as

$$\begin{aligned}\hat{\boldsymbol{\rho}}&=\left[\hat{\rho}_1,\hat{\rho}_2,\cdots,\hat{\rho}_{2N}\right]^{\mathrm{T}}\\&=\frac{1}{M}\sum_{i=1}^{M}\left(\left[\sqrt{B^i_{11}},\sqrt{B^i_{22}},\cdots,\sqrt{B^i_{2N2N}}\right]^{\mathrm{T}}\Big/\sqrt{B^i_{11}}\right),\end{aligned} \tag{38}$$

where $\hat{\rho}_1,\hat{\rho}_2,\cdots,\hat{\rho}_{2N}$ represent the estimated coefficients of gain errors.

3. Estimation of position error coefficients $f\left(\boldsymbol{z},\boldsymbol{\rho},\left[\Delta\hat{\boldsymbol{x}},\Delta\hat{\boldsymbol{y}}\right],\boldsymbol{\phi}\right)$

Third, the position error coefficients are optimized. Let $\boldsymbol{\psi}^i$=angle($\boldsymbol{B}^i$). When φ_1=0 we have

$$\psi^i_{1n}=\varphi_n+2\pi\xi,\ n=1,2,\cdots,2N, \tag{39}$$

where ξ is an integer. $2\pi\xi$ is the 2π phase ambiguous calibration term caused by the phase period. In other words, $\boldsymbol{\eta}^i$ as the first line of $\boldsymbol{\psi}^i$ after 2π phase ambiguous calibration can be used to obtain φ_n, where $\eta^1=\psi^1_{1n}$. η^i can be derived from the following.

Let $\Delta\psi^j_{1n}=\psi^{j+1}_{1n}-\psi^1_{1n},j=1,2.$ We have

$$\eta^{j+1}=\begin{cases}\psi^{j+1}_{1n}+2\pi, & \Delta\psi^j_{1n}<-\pi,\\ \psi^{j+1}_{1n}-2\pi, & \Delta\psi^j_{1n}>\pi,\\ \psi^{j+1}_{1n}, & \text{otherwise.}\end{cases} \tag{40}$$

Substituting Eq. (40) into Eq. (36) yields

$$\boldsymbol{\eta}^i=\begin{bmatrix}\phi_1\\ \phi_2\\ \vdots\\ \phi_{2N}\end{bmatrix}-\frac{2\pi}{\lambda}\left[\Delta\boldsymbol{x},\Delta\boldsymbol{y}\right]\begin{bmatrix}\sin\theta_i\\ \cos\theta_i\end{bmatrix},\ i=1,2,3. \tag{41}$$

Let $\Delta\boldsymbol{\eta}^j=\boldsymbol{\eta}^1-\boldsymbol{\eta}^{j+1},j=1,2.$ We have

$$\left[\Delta\boldsymbol{\eta}^1,\Delta\boldsymbol{\eta}^2\right]=\frac{2\pi}{\lambda}\left[\Delta\boldsymbol{x},\Delta\boldsymbol{y}\right]\cdot\begin{bmatrix}\sin\theta_2-\sin\theta_1 & \sin\theta_3-\sin\theta_1\\ \cos\theta_2-\cos\theta_1 & \cos\theta_3-\cos\theta_1\end{bmatrix}. \tag{42}$$

Thus, the estimated position error coefficients can be obtained by

$$\left[\Delta\hat{\boldsymbol{x}},\Delta\hat{\boldsymbol{y}}\right]=\frac{\lambda}{2\pi}\left[\Delta\boldsymbol{\eta}^1,\Delta\boldsymbol{\eta}^2\right]\cdot\begin{bmatrix}\sin\theta_2-\sin\theta_1 & \sin\theta_3-\sin\theta_1\\ \cos\theta_2-\cos\theta_1 & \cos\theta_3-\cos\theta_1\end{bmatrix}^{-1}. \tag{43}$$

According to $\left[\Delta\hat{\boldsymbol{x}},\Delta\hat{\boldsymbol{y}}\right]$, the position error matrix $\hat{\boldsymbol{H}}(\theta)$ can be reconstructed.

4. Estimation of phase error coefficients $f\left(\boldsymbol{z},\boldsymbol{\rho},\left[\Delta\boldsymbol{x},\Delta\boldsymbol{y}\right],\hat{\boldsymbol{\phi}}\right)$

Fourth, the phase error coefficients are optimized. Substituting Eq. (43) into Eq. (41), the phase error vector can be obtained as

$$\begin{aligned}\hat{\boldsymbol{\phi}}&=\left[\hat{\phi}_1,\quad \hat{\phi}_2,\quad \cdots,\quad \hat{\phi}_{2N}\right]^{\mathrm{T}}\\&=\frac{1}{3}\sum_{i=1}^{3}\left(\boldsymbol{\eta}^i+\frac{2\pi}{\lambda}\left[\Delta\hat{\boldsymbol{x}},\Delta\hat{\boldsymbol{y}}\right]\begin{bmatrix}\sin\theta_i\\ \cos\theta_i\end{bmatrix}\right),\end{aligned}\tag{44}$$

where $\hat{\phi}_1$, $\hat{\phi}_2$, …, $\hat{\phi}_{2N}$ indicate the estimated coefficients of the phase error. Thus, the gain-phase error matrix $\hat{\boldsymbol{G}}$ can be restructured based on the estimated gain error vector $\hat{\boldsymbol{\rho}}$ and the phase error vector $\hat{\boldsymbol{\phi}}$.

5. Convergence judgment

We have

$$J^{(l)}-J^{(l+1)}\le\sigma,\tag{45}$$

where σ is a small threshold. The iteration terminates when inequality (45) is established. Otherwise, l=l+1 and the algorithm returns to the first step to continue the calculation cycle until the optimal solution is found.

Finally, according to the subspace theory, the estimated mutual coupling matrix, gain-phase error matrix, and position error matrix are substituted into the MUSIC algorithm to estimate the DOAs of the incoherent sources.

3.2 Algorithm steps

From the above analysis, the comprehensive error calibration for the dual uniform circular array (CECDC for short) can be summarized as follows:

Step 1: By continuously rotating the antenna, three time-disjoint calibration sources θ_1, θ_2, and θ_3 are obtained, and the sample data matrix for each angle is captured.

Step 2: According to Eq. (17), the covariance matrix $\hat{\boldsymbol{R}}^i$ (i=1, 2, 3) is obtained, and then eigendecomposition is performed to obtain the corresponding noise subspace $\hat{\boldsymbol{E}}_N^i$ (i=1, 2, 3).

Step 3: initialization. Set the maximum number of iterations Υ, the number of iterations l=1, $\boldsymbol{G}^{(0)}$=$\boldsymbol{I}$, and $[\Delta\boldsymbol{x}^{(0)}, \Delta\boldsymbol{y}^{(0)}]$=[$\boldsymbol{0}$, $\boldsymbol{0}$].

Step 4: Calculate the mutual coupling error matrix $\hat{\boldsymbol{Z}}^{(l)}$ according to Eq. (33).

Step 5: Determine the gain-phase error matrix $\hat{\boldsymbol{G}}^{(l)}$ according to Eqs. (38) and (44), while the position error matrix $\hat{\boldsymbol{H}}^{(l)}(\theta)$ is obtained by Eq. (43).

Step 6: Substitute $\hat{\boldsymbol{Z}}^{(l)}$, $\hat{\boldsymbol{G}}^{(l)}$, and $\hat{\boldsymbol{H}}^{(l)}(\theta)$ into Eq. (19) to calculate the cost function J. If inequality (45) holds true, the algorithm ends. Otherwise, let l=l+1 and repeat steps 4–6 until the algorithm converges or l exceeds Υ.

The gain-phase errors, position errors, and mutual coupling errors gradually approach the true values with the gradual decrease in the cost function J. Subsequently, the estimated optimal error matrices are adopted in the MUSIC algorithm as known quantities to estimate DOAs of the impinging signals.

3.3 Discussion

1. Computational complexity analysis

Compared with the algorithm using multidimensional nonlinear joint search, the proposed algorithm has lower computational complexity. The parameters that need to be estimated are M signal angles, $2(2N-1)$ gain-phase error coefficients, $2(2N-1)$ position error coefficients, and $2(p+k+q-1)$ mutual coupling error coefficients. If the method using multidimensional nonlinear search is adopted to simultaneously estimate the unknown parameters, the search dimension is $2(4N+p+k+q-3)+M$. The amount of calculation is $O(N_\theta^M N_{\mathrm{G}}^{2(2N-1)} N_{\mathrm{P}}^{2(2N-1)} N_{\mathrm{Z}}^{2(p+k+q-1)})$, where N_θ, N_{G}, N_{P}, and N_{Z} represent the amount of computation required to estimate angles, gain-phase error coefficients, position error coefficients, and mutual coupling coefficients, respectively. Obviously, the computational complexity is very high. However, in this work, mutual coupling errors, gain-phase errors, and position errors are estimated in turn. Finally, the angles of signals are estimated. Although iterations are performed, there is no complex operation in each iteration. The total amount of calculation is $l\times O(N_\theta+N_{\mathrm{G}}+N_{\mathrm{P}}+N_{\mathrm{Z}})$. In contrast, the computational complexity of the proposed method is much lower than that of the method using multidimensional nonlinear joint search.

2. Analysis of fuzziness

Generally, there is a necessary but not sufficient condition for the uniqueness of solutions; that is, the number of unknown parameters should be smaller than that of independent equations. According to Friedlander and Weiss (1991), there are $2[2NM-M(M+1)/2]$ free parameters of the signal subspace and M+1 real eigenvalues in covariance matrix $\boldsymbol{R}$. The

unknown parameters in $\boldsymbol{R}$, however, include $2(p+k+q-1)$ unknown parameters in the mutual coupling matrix, $2(2N-1)$ unknown parameters in the gain-phase error matrix, $2(2N-1)$ unknown parameters in the position error matrix, as well as M unknown signals and one unknown noise power. Thus, the following holds true:

$$\begin{aligned}&2(p+k+q-1)+4(2N-1)+M+1\\&\le 2\left[2NM-M(M+1)/2\right]+M+1\\&\Rightarrow p+k+q\le 2NM-\frac{M^2+M}{2}-4N+3,\ M\ge 3.\end{aligned}\tag{46}$$

In addition, in Zhang et al. (2017), according to the array structure and the conclusion of many experiments, p, k, and q satisfy

$$\begin{cases}q<p\le\lceil N/2\rceil,\\1\le k\le p\le\lceil N/2\rceil,\\p+k+q\le N.\end{cases}\tag{47}$$

To summarize, the dual uniform circular array can realize unambiguous estimation when p, k, and q satisfy

$$\begin{cases}q<p\le\lceil N/2\rceil,\\1\le k\le p\le\lceil N/2\rceil,\\p+k+q\le N,\\p+k+q\le 2NM-\dfrac{M^2+M}{2}-4N+3,\ M\ge 3.\end{cases}\tag{48}$$

4 Simulation results

Several simulations have been carried out to demonstrate the performance of the proposed algorithm. The array structure is as shown in Fig. 1. The total number of array elements is 18; that is, both the inner and outer circular arrays have nine array elements. The radius of the inner circle is 0.5λ and that of the outer circle is λ, where λ is the wavelength. The gain errors satisfy the 80% normal distribution, while the phase errors satisfy the 50% distribution. The perturbation of the element position on the X and Y axes can be randomly selected in the range of $[-0.2\lambda, 0.2\lambda]$. Assume that the number of nonzero elements in $\boldsymbol{D}_1$ is p=3 and that the mutual coupling vector is $\boldsymbol{g}$=[1, 0.7821+0.2583j, 0.5476−0.2469j]. The number of nonzero elements in $\boldsymbol{D}_2$ is k=2, and the mutual coupling vector is $\boldsymbol{d}$=[1, 0.4982+0.2315j]. The number of nonzero elements in $\boldsymbol{B}$ is q=2 and the mutual coupling vector is $\boldsymbol{b}$=[0.6624+0.2503j, −0.5326+0.2369j]. Suppose there is an auxiliary source in the far field along direction 0°. The antenna is rotated twice continuously. The rotation angle interval between adjacent sources is 10°. Without loss of generality, an additive white Gaussian noise is added.

Experiment 1 (Estimation of error parameters) The gain-phase calibration error ε_{G}, position calibration error $\varepsilon_{x,y}$, and mutual coupling calibration error ε_{Z} can be defined as

$$\boldsymbol{\varepsilon}_{\mathrm{G}}=\left\|\hat{\boldsymbol{\delta}}-\boldsymbol{\delta}\right\|_{\mathrm{F}}\Big/\left\|\boldsymbol{\delta}\right\|_{\mathrm{F}},\tag{49}$$

$$\boldsymbol{\varepsilon}_{x,y}=\left\|\left[\Delta\hat{\boldsymbol{x}},\Delta\hat{\boldsymbol{y}}\right]-\left[\Delta\boldsymbol{x},\Delta\boldsymbol{y}\right]\right\|_{\mathrm{F}}\Big/\left\|\left[\Delta\boldsymbol{x},\Delta\boldsymbol{y}\right]\right\|_{\mathrm{F}},\tag{50}$$

$$\boldsymbol{\varepsilon}_{\mathrm{Z}}=\left\|\hat{\boldsymbol{z}}-\boldsymbol{z}\right\|_{\mathrm{F}}\Big/\left\|\boldsymbol{z}\right\|_{\mathrm{F}},\tag{51}$$

where $\boldsymbol{\delta}$ and $\hat{\boldsymbol{\delta}}$ denote the true and estimated values of the gain-phase error coefficients respectively, $[\Delta\boldsymbol{x}, \Delta\boldsymbol{y}]$ and $\left[\Delta\hat{\boldsymbol{x}},\Delta\hat{\boldsymbol{y}}\right]$ denote the true and estimated values of the position error coefficients respectively, and $\boldsymbol{z}$ and $\hat{\boldsymbol{z}}$ denote the true and estimated values of the mutual coupling coefficients respectively. Consider that the number of snapshots is 200 and that the SNR of the auxiliary source is 20 dB. The relationships between the cost function, gain-phase calibration errors, position calibration errors, mutual coupling coefficient calibration errors, and the number of iterations are shown in Figs. 2–5. The true and estimated values of the three different kinds of error coefficients are compared in Tables 1–3.

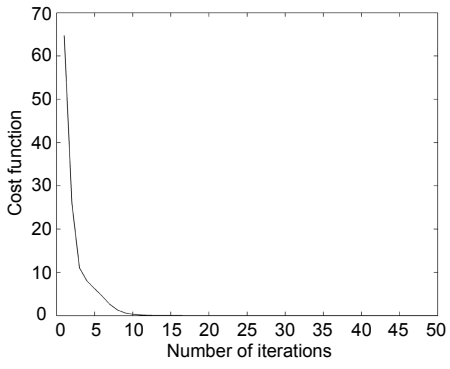

Fig. 2 The cost function vs. the number of iterations

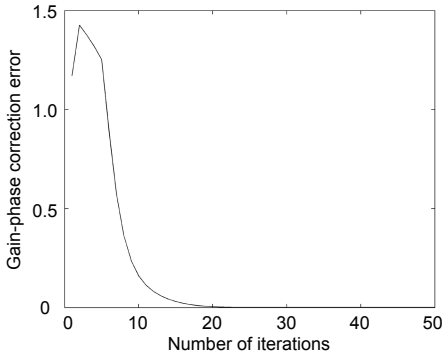

Fig. 3 The gain-phase correction error vs. the number of iterations

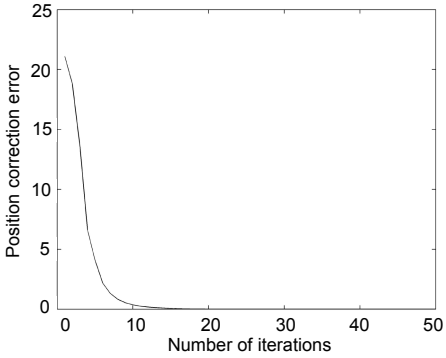

Fig. 4 The position correction error vs. the number of iterations

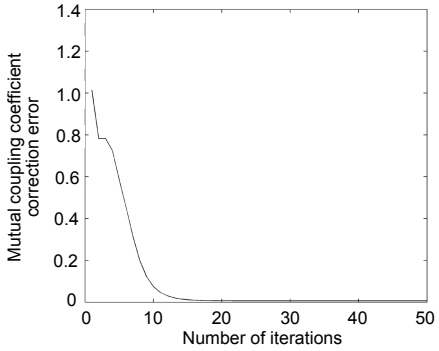

Fig. 5 The mutual coupling coefficient correction error vs. the number of iterations

Fig. 2 shows that the proposed algorithm converges very fast at the beginning. When the number of iterations exceeds 15, the algorithm converges to a stable value. This verifies that the proposed algorithm has good convergence. Figs. 3–5 show that the calibration errors of various error coefficients gradually approach 0 as the number of iterations increases. Tables 1–3 further verify that the proposed algorithm can estimate the three kinds of error coefficients very accurately.

Table 1 Estimation results of the gain-phase error coefficients

Array element	True value	Estimated value
1	1.0000+0.0000j	1.0000−0.0000j
2	1.5683+0.0688j	1.5683+0.0688j
3	1.7283+0.5418j	1.7279+0.5436j
4	1.2011+0.3710j	1.2007+0.3724j
5	1.5610+0.4357j	1.5613+0.4325j
6	1.1215+0.4905j	1.1211+0.4917j
7	1.1477+0.1371j	1.1476+0.1417j
8	1.1247+0.0342j	1.1246+0.0362j
9	1.3688+0.5268j	1.3693+0.5245j
10	1.2533+0.3077j	1.2524+0.3118j
11	1.1364+0.1370j	1.1369+0.1351j
12	1.2003+0.4088j	1.2000+0.4106j
13	1.4402+0.5240j	1.4413+0.5159j
14	1.3211+0.2103j	1.3198+0.2195j
15	1.0758+0.3947j	1.0747+0.3999j
16	1.2229+0.5507j	1.2247+0.5462j
17	1.5617+0.7905j	1.5600+0.7944j
18	1.1432+0.5861j	1.1443+0.5859j

Table 2 Estimation results of the position error coefficients

Array element	*X* axis		*Y* axis	
	True	Estimated	True	Estimated
1	0.0000	0.0000	0.0000	0.0000
2	−0.1298	−0.1300	−0.1442	−0.1443
3	0.1367	0.1368	0.1397	0.1392
4	0.1250	0.1250	−0.0663	−0.0679
5	−0.1056	−0.1060	0.1180	0.1174
6	−0.1040	−0.1040	−0.0986	−0.0994
7	−0.1549	−0.1549	−0.0573	−0.0578
8	−0.1150	−0.1149	0.1804	0.1800
9	0.1062	0.1063	0.1110	0.1111
10	−0.0630	−0.0629	−0.1316	−0.1323
11	−0.1347	−0.1345	0.1888	0.1877
12	−0.0197	−0.0195	0.0294	0.0295
13	0.0913	0.0911	0.1251	0.1250
14	0.1615	0.1615	0.0522	0.0522
15	−0.1846	−0.1850	−0.1584	−0.1586
16	−0.1539	−0.1539	0.1195	0.1194
17	0.1305	0.1304	0.1081	0.1083
18	−0.1916	−0.1916	−0.1374	−0.1372

Table 3 Estimation results of the mutual coupling coefficients

	True value	Estimated value
$\boldsymbol{g}(2)$	0.7821+0.2583j	0.7822+0.2583j
$\boldsymbol{g}(3)$	−0.5476+0.2469j	−0.5477+0.2469j
$\boldsymbol{b}(1)$	0.6624−0.2503j	0.6624−0.2504j
$\boldsymbol{b}(2)$	−0.5326+0.2369j	−0.5326+0.2369j
$\boldsymbol{c}(2)$	0.4982+0.2315j	0.4982+0.2314j

Experiment 2 (1D spatial spectrum) The angular estimation performance of the array after comprehensive error calibration is analyzed in this experiment. Assume that three independent signal sources (SNR=15 dB) with the same power impinge on the array from directions −5°, 0°, and 5°, respectively. The number of snapshots is 300. Fig. 6 shows the comparison of the spatial spectrum at different numbers of iterations using uncalibrated MUSIC, the algorithm in Ng and See (1996), and CECDC when the SNR of the auxiliary source is 10 dB and 20 dB.

Fig. 6 shows that the uncalibrated MUSIC fails when the comprehensive range of errors exists. CECDC and the algorithm in Ng and See (1996) can successfully estimate the three signals, and the performance of CECDC is better. The spectrum peak of the signals becomes sharper with the increasing SNR of the auxiliary source, which can prove that CECDC performs better and better. Note that the performance of CECDC is basically stable when the number of iterations exceeds 20. This is consistent with the conclusion in Experiment 1.

Experiment 3 (Effect of calibration sources on the performance of DOA estimation) The estimated performances of CECDC and the algorithms in Hu (2009) and Wang (2011) are compared when mutual coupling errors and gain-phase errors are present (Fig. 7). The DOA estimation accuracy is measured by the root mean square error (RMSE), defined as

$$\theta_{\mathrm{RMSE}}=\sqrt{\sum_{k=0}^{M_{\mathrm{c}}}\sum_{i=1}^{M}\left(\hat{\theta}_{i,k}-\theta_i\right)^2\Big/(M_{\mathrm{c}}M)}, \tag{52}$$

where M_{c} is the number of Monte Carlo trials. Suppose the number of snapshots is 512. SNR varies from 5 to 31 dB, with an interval of 2 dB. One hundred Monte Carlo simulations are carried out to analyze the relationship between RMSE and SNR of the calibration sources (Fig. 7a). SNR is 10 dB. The number of snapshots varies from 10 to 510, with an interval of 50. The relationship between RMSE and the number of snapshots is shown in Fig. 7b. RMSE vs. the angle bias of the calibration source is shown in Fig. 7c when SNR is 10 dB and the number of snapshots is 300.

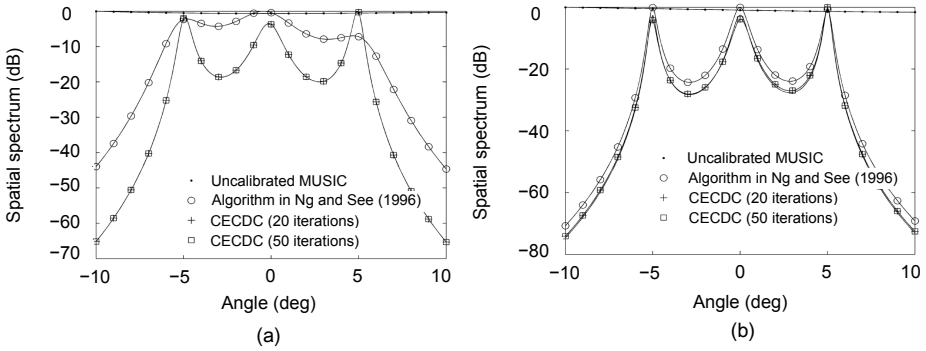

Fig. 6 One-dimensional spatial spectrum: (a) SNR=10 dB; (b) SNR=20 dB

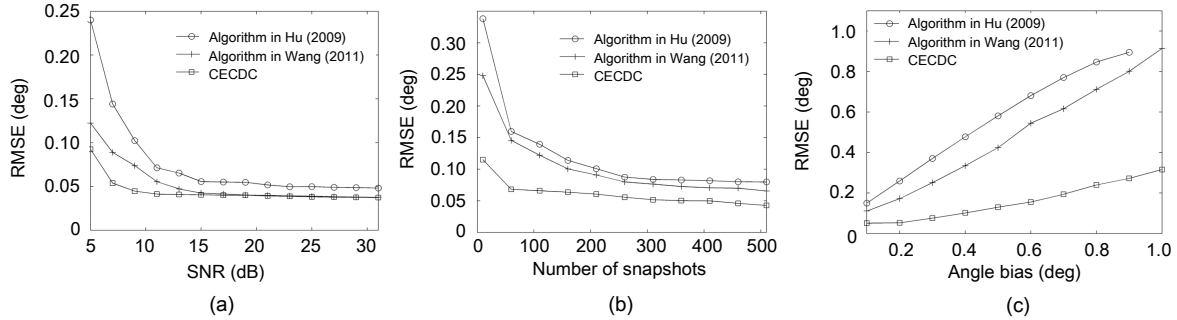

Fig. 7 The effect of calibration sources on estimation performance: (a) RMSE vs. SNR; (b) RMSE vs. the number of snapshots; (c) RMSE vs. angle bias

Figs. 7a and 7b show that the RMSE of the three algorithms gradually decreases with the increase of SNR or the number of snapshots. CECDC has better estimation accuracy than the algorithms in Hu (2009) and Wang (2011). Fig. 7c shows that when the auxiliary source is biased, the performance of CECDC is slightly affected, while the performances of the algorithms in Hu (2009) and Wang (2011) are seriously degraded. When the angle bias exceeds 0.9°, the algorithm in Hu (2009) fails completely. Experiment 3 verifies that CECDC performs better, especially for the case in which the auxiliary source is not known precisely.

Experiment 4 (Estimation accuracy corresponding to different mutual coupling errors, gain-phase errors, and position errors) The estimation accuracy under different errors is analyzed in this experiment. The RMSE of mutual coupling errors, position errors, gain errors, and phase errors can be defined as

$$\boldsymbol{e}_z=\frac{1}{\|\boldsymbol{Z}\|_{\mathrm{F}}}\sqrt{\left(\sum_{j=1}^{M_{\mathrm{c}}}\left\|\boldsymbol{Z}-\hat{\boldsymbol{Z}}_j\right\|_{\mathrm{F}}^2\right)\Big/M_{\mathrm{c}}}\times100\%, \tag{53}$$

$$\boldsymbol{e}_{[\Delta\boldsymbol{x},\Delta\boldsymbol{y}]}=\frac{1}{\|[\Delta\boldsymbol{x},\Delta\boldsymbol{y}]\|_{\mathrm{F}}}\cdot\sqrt{\left(\sum_{j=1}^{M_{\mathrm{c}}}\left\|[\Delta\boldsymbol{x},\Delta\boldsymbol{y}]-[\Delta\hat{\boldsymbol{x}},\Delta\hat{\boldsymbol{y}}]_j\right\|_{\mathrm{F}}^2\right)\Big/M_{\mathrm{c}}}\times100\%, \tag{54}$$

$$\boldsymbol{e}_\rho=\frac{1}{\|\boldsymbol{\rho}\|_{\mathrm{F}}}\sqrt{\left(\sum_{j=1}^{M_{\mathrm{c}}}\left\|\boldsymbol{\rho}-\hat{\boldsymbol{\rho}}_j\right\|_{\mathrm{F}}^2\right)\Big/M_{\mathrm{c}}}\times100\%, \tag{55}$$

$$\boldsymbol{e}_\phi=\frac{1}{\|\boldsymbol{\phi}\|_{\mathrm{F}}}\sqrt{\left(\sum_{j=1}^{M_{\mathrm{c}}}\left\|\boldsymbol{\phi}-\hat{\boldsymbol{\phi}}_j\right\|_{\mathrm{F}}^2\right)\Big/M_{\mathrm{c}}}\times100\%. \tag{56}$$

Assume that three time-disjoint sources are in the far field with directions −10°, 0°, and 10°. When only the mutual coupling errors exist, the RMSEs of mutual coupling errors by the proposed algorithm and the algorithms in Lin and Yang (2006) and Ye and Liu (2008) are compared in Fig. 8. The simulation conditions are kept unchanged. When only position errors exist, the RMSEs of position errors by the proposed algorithm and the algorithms in Chen (2009) and Yuan et al. (2014) are compared in Fig. 9. Similarly, when the gain-phase errors exist alone, Figs. 10 and 11 show the RMSEs of gain errors and phase errors, respectively.

Experimental results show that the estimation accuracy of the proposed algorithm becomes better and better with the increase of SNR and the number of snapshots. When mutual coupling errors exist alone, the estimation accuracy of the proposed algorithm is better than that of the algorithms proposed by Lin and Yang (2006) and Ye and Liu (2008), especially at low SNR. When position errors or gain-phase errors exist alone, our proposed algorithm has higher estimation accuracy and better calibration performance than the methods in Chen (2009) and Yuan et al. (2014).

Experiments show that the proposed algorithm is also applicable to single error calibration.

Experiment 5 (2D spatial spectrum) The performance of 2D angle estimation is investigated in this experiment. Suppose that there are two equal power incoherent signals in the far field with directions (30°, 20°) and (45°, 40°). The number of snapshots is 300 and the SNR is 10 dB. Under the condition where three kinds of errors coexist, Figs. 12–14 show the 2D spatial spectrum of uncalibrated MUSIC, the algorithm in Ng and See (1996), and CECDC.

Figs. 12–14 show that the uncalibrated MUSIC fails in 2D angle estimation while the algorithm in Ng and See (1996) and CECDC form two peaks in the signal directions. The two peaks formed by CECDC are sharper. The exact angles of the two signals are more clearly measured from the corresponding contour map in Figs. 13b and 14b. The signal directions estimated by the proposed algorithm are more accurate. This demonstrates that the proposed algorithm performs well in the calibration of gain-phase errors, position errors, and mutual coupling errors. It can effectively and comprehensively deal with the errors in the dual uniform circular array.

Note that the convergence of the algorithm can be guaranteed because the cost function is reduced in each iteration. Moreover, the cost function is always non-negative. Simulation results show that the algorithm can converge to the optimal solution, and the estimated value of each error is basically the same as the real value. However, in actual applications, there are many factors affecting array calibration, such as the environment, weather, and the limited number of snapshots. Usually, the stable value of algorithm convergence in reality is larger than that in the simulations. Yet, this does not affect the effective convergence of the cost function.

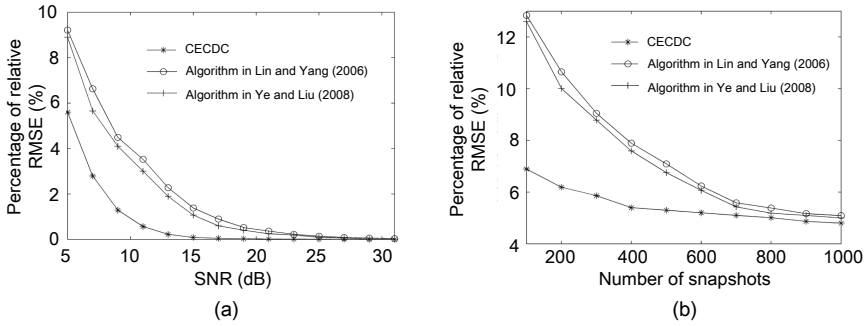

Fig. 8 Relative RMSE of mutual coupling errors: (a) relative RMSE vs. SNR (*L*=300); (b) relative RMSE vs. the number of snapshots (SNR=10 dB)

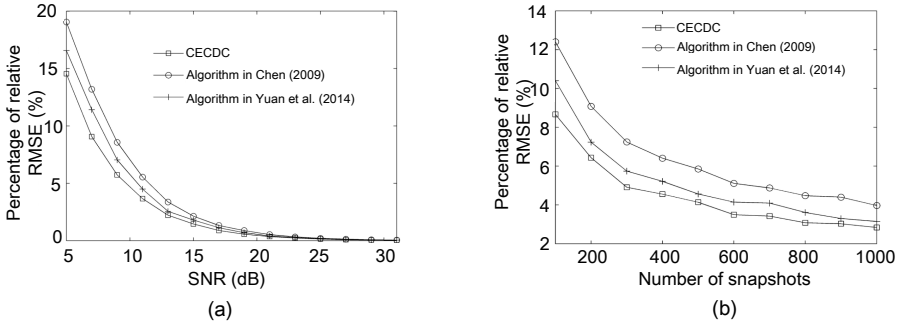

Fig. 9 Relative RMSE of position errors: (a) relative RMSE vs. SNR (*L*=300); (b) relative RMSE vs. the number of snapshots (SNR=10 dB)

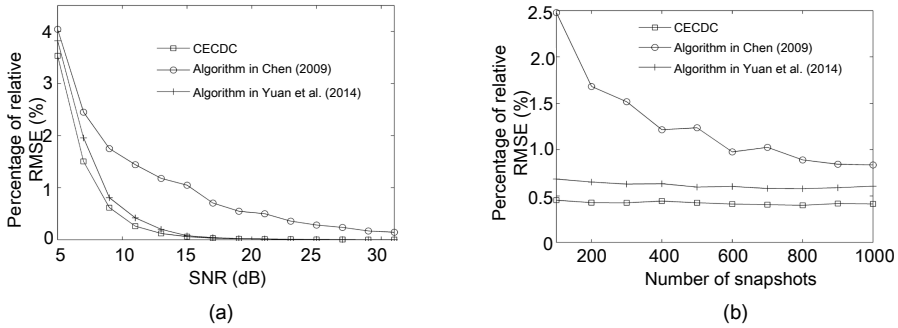

Fig. 10 Relative RMSE of gain errors: (a) relative RMSE vs. SNR (*L*=300); (b) relative RMSE vs. the number of snapshots (SNR=10 dB)

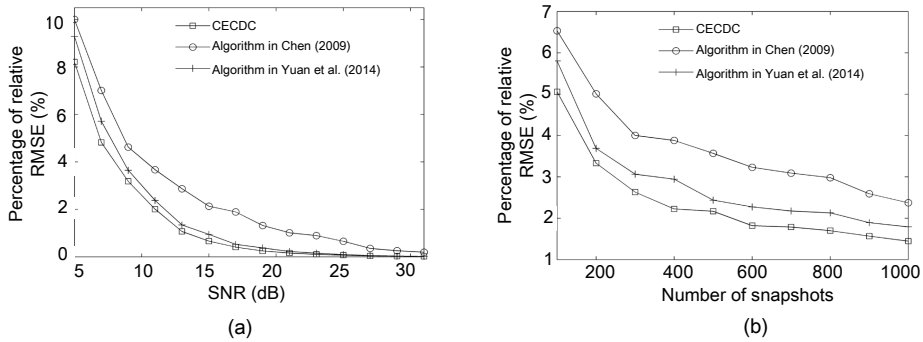

Fig. 11 Relative RMSE of phase errors: (a) relative RMSE vs. SNR (*L*=300); (b) relative RMSE vs. the number of snapshots (SNR=10 dB)

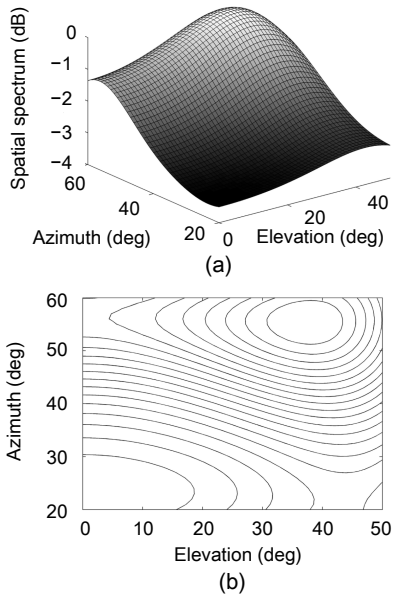

Fig. 12 Uncalibrated MUSIC algorithm: (a) 2D spatial spectrum; (b) counter map

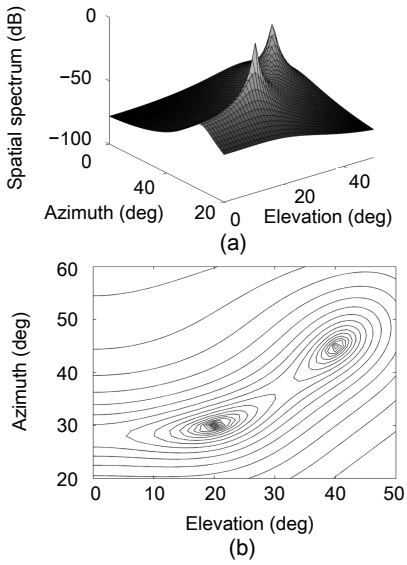

Fig. 13 Algorithm in Ng and See (1996): (a) 2D spatial spectrum; (b) counter map

5 Conclusions

In this study, aimed at the situation where gain-phase errors, position errors, and mutual coupling errors coexist in a dual uniform circular array, a new method is proposed to comprehensively deal with the errors and estimate the DOAs of incoherent sources. The situation where three kinds of errors exist at the same time is more in line with reality. During mutual coupling estimation, the array structure of the dual uniform circle array is fully used. The cyclic banded symmetric Toeplitz characteristics of the partitioned mutual coupling matrices ($\boldsymbol{D}_1$, $\boldsymbol{D}_2$, and $\boldsymbol{B}$) are used to decouple the angles and the mutual coupling coefficients. In the estimation of gain-phase errors and position errors, the signal phase matrix is constructed, which effectively eliminates the phase influence caused by the delay of the signal reaching the antenna. Compared with the algorithm using multidimensional nonlinear search, the proposed algorithm simplifies the computation. Moreover, the new method does not require additional auxiliary elements. Simulation results show that the algorithm can converge effectively. It can estimate the DOAs of incoherent sources and the coefficients of three kinds of errors well. It is of strong significance in the comprehensive calibration of errors in reality.

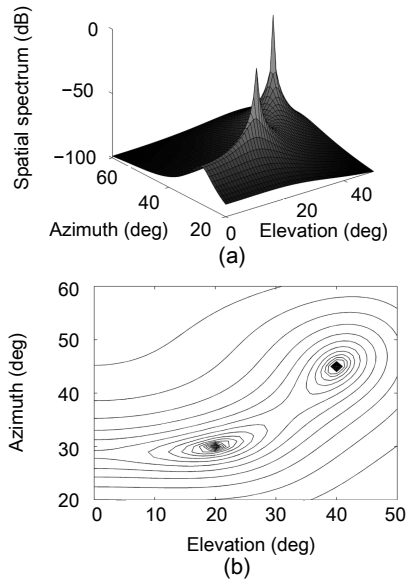

Fig. 14 CECDC algorithm: (a) 2D spatial spectrum; (b) counter map

Compliance with ethics guidelines

Jia-jia ZHANG, Hui CHEN, Song XIAO, and Meng-yu NI declare that they have no conflict of interest.

References

Belfiori F, Monni S, van Rossum W, et al., 2012. Antenna array characterisation and signal processing for an FM radio-based passive coherent location radar system. *IET Radar Sonar Nav*, 6(8):687-696. https://doi.org/10.1049/iet-rsn.2011.0401

Chen H, 2009. Research on Some Aspects of High Resolution Direction of Arrival Estimation. PhD Thesis, Huazhong University of Science and Technology, Wuhan, China (in Chinese).

Cheng F, Gong ZP, Zhang C, et al., 2017. A new rotation measurement-based method for array gain-phase errors calibration. *J Electron Inform Technol*, 39(8):1899-1905 (in Chinese). https://doi.org/10.11999/JEIT161058

Friedlander B, Weiss AJ, 1991. Direction finding in the presence of mutual coupling. *IEEE Trans Antenn Propag*, 39(3):273-284. https://doi.org/10.1109/8.76322

Guo YD, Zhang YS, Tong NN, et al., 2017. Angle estimation and self-calibration method for bistatic MIMO radar with transmit and receive array errors. *Circ Syst Signal Process*, 36(4):1514-1534. https://doi.org/10.1007/s00034-016-0365-9

Hu XQ, 2009. Basis Study on the Application of Super-Resolution Spatial Spectrum Estimation Technique. PhD Thesis, National University of Defense Technology, Changsha, China (in Chinese).

Jia YK, Bao Z, Wu H, 1996. A new calibration technique with signal sources for position, gain and phase uncertainty of sensor array. *Acta Electron Sin*, 24(3):47-52 (in Chinese).

Jin R, Li QX, Dong J, et al., 2010. Receiving array calibration method for amplitude and phase errors at low SNR. *J Microw*, 26(3):68-72, 82 (in Chinese).

Li WX, Lin JZ, Zhang Y, et al., 2016. Joint calibration algorithm for gain-phase and mutual coupling errors in uniform linear array. *Chin J Aeronaut*, 29(4):1065-1073. https://doi.org/10.1016/j.cja.2016.04.018

Lin M, Yang L, 2006. Blind calibration and DOA estimation with uniform circular arrays in the presence of mutual coupling. *IEEE Antenn Wirel Propag Lett*, 5(1):315-318. https://doi.org/10.1109/LAWP.2006.878898

Liu S, Yang LS, Yang SZ, 2016. Robust joint calibration of mutual coupling and channel gain/phase inconsistency for uniform circular array. *IEEE Antenn Wirel Propag Lett*, 15:1191-1195. https://doi.org/10.1109/LAWP.2015.2499280

Ng BC, See CMS, 1996. Sensor array calibration using a maximum-likelihood approach. *IEEE Trans Antenn Propag*, 44(6):827-835. https://doi.org/10.1109/8.509886

Sellone F, Serra A, 2007. A novel online mutual coupling compensation algorithm for uniform and linear arrays. *IEEE Trans Signal Process*, 55(2):560-573. https://doi.org/org/10.1109/TSP.2006.885732

Wang D, 2011. Research on the Errors Calibration Techniques in the Array Signal Processing. PhD Thesis, PLA Information Engineering University, Zhengzhou, China (in Chinese).

Wang D, 2015. Improved active calibration algorithms in the presence of channel gain/phase uncertainties and sensor mutual coupling effects. *Circ Syst Signal Process*, 34(6):1825-1868. https://doi.org/10.1007/s00034-014-9926-y

Wang D, Wu Y, 2015. The multiplicative array errors calibration algorithms in the presence of multipath. *Sci China Inform Sci*, 45(2):270-288 (in Chinese). https://doi.org/10.1360/N112013-00060

Wang M, Ma XC, Yan SF, et al, 2015. An auto-calibration algorithm for uniform circular array with unknown mutual coupling. *IEEE Antenn Wirel Propag Lett*, 15(6):12-15. https://doi.org/10.1109/LAWP.2015.2425423

Wang YL, Chen H, Peng YN, et al., 2004. Theory and Algorithms of Spatial Spectrum Estimation. Tsinghua University Press, Beijing, China, p.419-443 (in Chinese).

Wu N, Qu ZY, Si WJ, et al., 2016. DOA and polarization estimation using an electromagnetic vector sensor uniform circular array based on the ESPRIT algorithm. *Sensors*, 16(12):2109. https://doi.org/10.3390/s16122109

Ye ZF, Liu C, 2008. On the resiliency of MUSIC direction finding against antenna sensor coupling. *IEEE Trans Antenn Propag*, 56(2):371-380. https://doi.org/10.1109/TAP.2007.915461

Yuan ZY, Niu YM, Yang G, et al., 2014. A calibration method for sensor gain/phase and position errors of array antenna. *J Electron Inform Technol*, 36(9):2232-2237 (in Chinese). https://doi.org/10.3724/SP.J.1146.2013.01807

Zhang JJ, Chen H, Li S, et al., 2017. Self calibration of mutual coupling for dual uniform circular array. *J Electron Inform Technol*, 39(7):1539-1545 (in Chinese). https://doi.org/10.11999/JEIT161137

Zhang JJ, Chen H, Ji ZY, et al., 2018. Direction characteristics for dual circular array. *Chin J Radio Sci*, 33(1):93-104 (in Chinese). https://doi.org/10.13443/j.cjors.2017042501